Properties of the kinetic energy budgets in wall-bounded turbulent flows

Ang Zhou and Joseph Klewicki

Phys. Rev. Fluids **1**, 044408 — Published 16 August 2016
DOI: 10.1103/PhysRevFluids.1.044408

Properties of the kinetic energy budgets in wall-bounded turbulent flows

Ang Zhou* and Joseph Klewicki†
Department of Mechanical Engineering, University of New Hampshire, Durham, New Hampshire 03824, USA
(Dated: June 23, 2016)

Available high quality numerical simulation data are used to investigate and characterize the kinetic energy budgets for fully-developed turbulent flow in pipes and channels, and in the zero-pressure gradient turbulent boundary layer. The mean kinetic energy equation in these flows is empirically and analytically shown to respectively exhibit the same four-layer leading order balance structure as the mean momentum equation. This property of the mean kinetic energy budget provides guidance on how to group terms in the more complicated turbulence and total kinetic energy budgets. Under the suggested grouping, the turbulence budget shows either a two or three layer structure (depending on channel or pipe versus boundary layer flow), while the total kinetic energy budget exhibits a clear four-layer structure. These layers, however, differ in position and size and exhibit variations with friction Reynolds number (δ^+) that are distinct from the layer structure associated with the mean dynamics. The present analyses indicate that each of the four layers is characterized by a predominance of a reduced set of the grouped terms in the governing equation. The width of the third layer is mathematically reasoned to scale like $\delta^+ - \sqrt{\delta^+}$ at finite Reynolds numbers. In the boundary layer the upper bounds of both the second and third layers convincingly merge under this normalization, as does the width of the third layer. This normalization also seems to be valid for the width of the third layer in pipes and channels, but only for $\delta^+ > 1000$. The leading order balances in the total kinetic energy budget are shown to arise from a non-trivial interweaving of the mean and turbulence budget contributions with distance from the wall.

I. INTRODUCTION

Wall-bounded turbulent flows at high Reynolds numbers have become an increasingly active area of research over the past several decades [1–3]. Here, scaling analyses are used to investigate Reynolds number dependencies and their physical and mathematical ramifications. When the Reynolds number is sufficiently large, there is a region where the streamwise mean velocity profile exhibits a logarithmic variation, e.g., [4, 5]. More recent studies indicate that the variance of the streamwise velocity fluctuations as well as their higher order even moments also exhibit a logarithmic decay over nominally the same domain [6, 7]. Consistent with classical notions, this domain is sufficiently remote from boundary condition effects, and the dynamics on this domain are dominated by inertial momentum transport mechanisms. This inertial domain is also associated with a self-similar structure admitted by the mean dynamical equation [8], and consistently, other statistical measures evidence self-similarity here as well [9, 10]. In accord with self-similarity, analysis of the mean momentum equation indicates that the inertial domain coincides with where the wall-normal derivative of the widths of an intrinsic hierarchy of scaling layers approaches a constant as the Reynolds number becomes large [11]. The present study complements these mean dynamics based analyses by clarifying the average structure of the energy budgets in turbulent channel, pipe, and boundary layer flows. This is accomplished by elucidating the leading order balances of terms in the kinetic energy budgets, and contrasting these with the leading balances exhibited by the mean momentum equation.

The traditional description of turbulent wall-flow structure has direct connection to the properties of the mean velocity profile [12]. This profile is typically made non-dimensional using inner variables, u_τ and ν, where $u_\tau = \sqrt{\tau_w/\rho}$ is the friction velocity, τ_w is the mean wall shear stress and ν is the kinematic viscosity. With this description, the viscous sublayer flow, $0 \lesssim y^+ \lesssim 5$, is dominated by the effects of viscosity and characterized by a linear mean profile. In the buffer layer, $5 \lesssim y^+ \lesssim 30$, the viscous and Reynolds stresses are both dynamically significant, and the profile transitions from linear to approximately logarithmic. Under the mean profile description, these two layers are associated with the direct effect of viscosity, and their thickness remains a fixed number of viscous lengths independent of Reynolds number. Consistently, the velocity increments across these layers are a fixed number in inner units. In the third classical layer, the mean velocity has a logarithmic variation from near $y^+ \simeq$ *constant* to $y/\delta \simeq 0.2$. The dynamics here are seen to be dominated by the inertial effects of the turbulence. In the wake layer, $0.2 \lesssim y/\delta \lesssim 1$, mean inertia (or mean pressure gradient) and turbulent inertia comprise the predominant dynamical mechanisms. The logarithmic and wake layers grow at a rate proportional to δ with their velocity increments approaching a fixed fraction of U_∞ as $\delta^+ \to \infty$ [13, 14].

Efforts to describe kinetic energy and kinetic energy equation behaviors in turbulent wall-flows arguably began in earnest with the experimental studies by Laufer and Klebanoff [15–17]. As remains the case for physical

* zhouang48@gmail.com.
† Also at the Department of Mechanical Engineering, University of Melbourne, Victoria 3010 Australia.; joe.klewicki@unh.edu or klewicki@unimelb.edu.au.

experiments today, analyses were conducted without the benefit of the comprehensive quantification of terms that is now provided by direct numerical simulations, DNS. These earlier descriptions were generally given within the context of the traditional layer structure just described, and often (but not exclusively) focused on the turbulence kinetic energy (TKE). These early measurements revealed that not all terms in the TKE budget are leading order across the entire flow, and in particular the production and dissipation terms were found to nominally comprise the leading balance across the logarithmic layer. Guided by such measurements, subsequent analyses and interpretations were made within the context of the budget equations. Using his attached eddy concepts, Townsend [18] surmised that in the logarithmic layer the streamwise and spanwise velocity fluctuation contributions to the TKE are, in the asymptotic limit, given by functions that logarithmically decrease with distance from the wall, with the wall-normal velocity fluctuation contribution approaching a constant. Townsend further described equilibrium boundary layer energy transport as consisting of an inward flux of mean kinetic energy that is coincident with an outward flux of turbulence energy, and with the primary conversion of mean to turbulence kinetic energy occurring in the logarithmic layer and below. Near the outer edge, he surmised that the approximate balance is between the advection and turbulent transport terms, and thus is inviscid at leading order. The approximate balance between dissipation in the logarithmic layer is often employed in wall-turbulence scaling arguments, and is regularly used to explain the existence of a logarithmic mean profile, e.g., [12, 14].

Studies over the past decade have used the properties of the mean momentum equation to discern Reynolds number dependence, scaling and dynamics [3, 19]. In contrast to the traditional layer structure described above, these analyses reveal a different four-layer structure for Reynolds numbers above the transitional regime [20]. Denoted by layers I-IV, this structure was revealed and characterized by considering the relative magnitudes of the terms in the mean momentum equation. A sketch of this layer structure at any given post-transitional Reynolds number is presented in Fig. 1.

Layer I essentially retains the character of the viscous sublayer, and is a region where the viscous stress gradient nominally balances the mean pressure gradient in the channel/pipe or mean advection in the boundary layer. In this layer, there exists a perturbed sheet-like distribution of negative spanwise vorticity in the $x - z$ plane, and these perturbations motivate the evolution of motions out of layer I. (Note that x is in flow direction and y is the wall-normal coordinate). In layer II, the ratio of the viscous stress gradient to the Reynolds stress gradient is close to -1, and thus these two terms comprise the leading order balance. Layer II is associated with the three-dimensionalization of the vorticity field, and a reduction in the scale of the vortical motions relative to those characteristic of the velocity field [21]. Across layer III, the Reynolds stress attains its maximum value, and thus its gradient changes sign. This is associated with a balance breaking and exchange of dominant terms [22]. Here, all terms are nominally of the same order of magnitude. The last layer (layer IV) is characterized by a loss of the leading order viscous stress gradient term, and for greater wall-normal distances the Reynolds stress gradient is balanced by the mean pressure gradient or mean advection term. In contrast to layer II, the vortical motions become uncorrelated with the vorticity field near the wall, and form into slender vortical fissures [21].

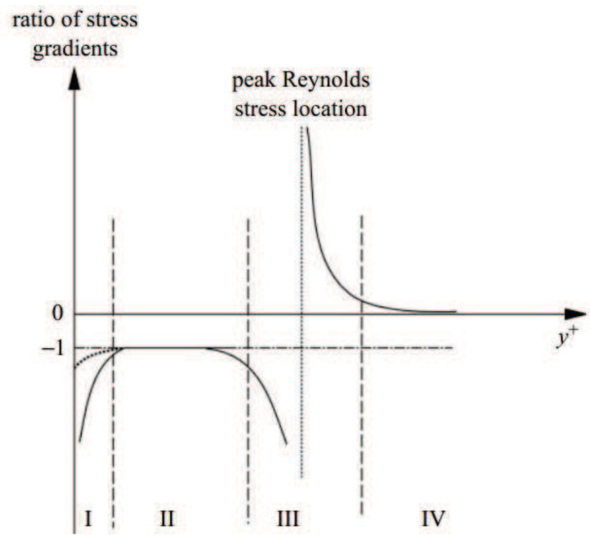

FIG. 1. Sketch of the ratio of the viscous stress gradient to the Reynolds stress gradient in boundary layer, pipe and channel ows at any given Reynolds number. The dotted line in layer I is for a boundary layer, and the solid line is for a pipe or channel.

As expected, layer I and layer IV respectively comply with inner and outer scaling. However, an intermediate length scale, i.e., $\sqrt{\nu\delta/u_\tau}$, is empirically observed and analytically shown to characterize the other two layers, with their thicknesses respectively given by $3 \lesssim y^+_{II} \lesssim 1.6\sqrt{\delta^+}$ and $1.6\sqrt{\delta^+} \lesssim y^+_{III} \lesssim 2.6\sqrt{\delta^+}$. The velocity increment across layer II remains about one half of U_∞, independent of δ^+, while there is only about a $1.0u_\tau$ increment across layer III [20].

Of course, the interest in Reynolds number effects also extends to the TKE equation. As such, an equation based characterization of the leading balances, similar to that just given for the mean momentum equation, is desired. The difficulties in obtaining accurate experimental measurements of the relevant quantities postponed the accurate determination of each term in the TKE budget until the advent of DNS. Since the early DNS of Mansour *et al* [23], numerous other studies have explored the behavior of the terms in the TKE equation [24–27]. From these studies, it is probably safe to surmise that a clear scaling structure to the TKE budget (and associated Reynolds stress budgets) has yet to emerge [28].

Some general behaviors are, however, known to hold. At the wall the dissipation term is maximal and is balanced with the viscous diffusion term. Near the wall, the dissipation term balances with the sum of the viscous diffusion and pressure diffusion terms. Moving away from the wall, the pressure diffusion term is small compared to other terms, and the turbulent diffusion term becomes important. This term is positive near the wall, but negative for $8 \lesssim y^+ \lesssim 30$. It thus plays a role in transporting TKE towards the wall. In the region $y^+ \gtrsim 30$, however, the balance is nominally composed of the production and dissipation terms. It is rationally expected that both the dissipation term, which is dependent on small scale structure, and the turbulent diffusion term, which is typically associated with larger scales, are sensitive to Reynolds number via the effects of scale separation. Also, above the traditional buffer layer, most terms in the TKE transport equation scale reasonably well with u_τ^3/δ. Within the viscous and buffer layers, inner-normalization, u_τ^4/ν, seems to apply, but the inner scaling works poorly very close to the wall, especially for the dissipation and pressure-related terms. The former is attributed to the effect of the large scale motions, and the latter is due to the scaling of pressure itself [28].

The above and similar descriptions of kinetic energy transport are referenced to the traditional layer structure. The relevance of this structure to scaling the flow field energetics is, however, not well-established. Given this, the present study mimics the more recent approach used in the analysis of the mean momentum equation [20]. This approach is used to explore the mean, turbulence, and total kinetic energy balances in planar channels, circular pipes, and flat plate boundary layer flows. Here we note that the analysis of section II A 3 reveals that the leading order layer structure of the mean kinetic energy balance is identical to that of the mean momentum balance, while for Reynolds numbers available to DNS, the profiles of the terms in the turbulence kinetic energy equations are very similar in pipes and channels. The present analyses indicate that there exists a four-layer structure to the total kinetic energy budget equation, with the property that in each of these layers a balance occurs between a subset of the relevant terms. This layer structure is, however, shown to be distinct from the layer structure of the mean momentum balance. The Reynolds number dependent scaling of the thickness of each layer is empirically quantified using DNS data, and for one layer (layer ii) is also analytically reasoned. The physical processes associated with each layer and their connections to the kinetic energy balance for the mean flow and turbulence are also discussed and clarified.

II. KINETIC ENERGY BUDGETS

In the following, x denotes the streamwise direction, with the wall-normal direction given by y. Upper-case letters or angle brackets denote the averaged quantities, and lower-case letters indicate fluctuations about the mean. The x, y and z velocity components are given by variants of u, v and w, respectively, and δ is used to denote the boundary layer thickness, pipe radius, or half channel height.

A. Mean kinetic energy budgets

Consideration of the mean kinetic energy balance reveals an important connection to the structure of the mean dynamics. With the Reynolds stress denoted by $\tau_{ij}^R = -\langle u_i u_j \rangle$, in a Cartesian system the balance equation for the mean kinetic energy, $E = 1/2\,(U_i U_i)$, is

$$\frac{\partial}{\partial t}\left(\frac{1}{2}U_iU_i\right)+U_k\frac{\partial}{\partial x_k}\left(\frac{1}{2}U_iU_i\right) = -\frac{1}{\rho}\frac{\partial}{\partial x_i}\left(U_iP\right) +\nu U_i\frac{\partial^2 U_i}{\partial x_k\partial x_k}+U_i\frac{\partial}{\partial x_k}\tau_{ij}^R, \tag{1}$$

where the conventions of indicial notation are taken to hold.

1. *Fully developed turbulent channel and pipe flows*

Statistically stationary and fully developed turbulent flow in a planar channel or circular pipe with smooth walls is considered. Since this flow is both planar (axisymmetric) and fully developed, derivatives of averaged quantities with respect to x and z are zero, and such mean quantities are solely a function of y, e.g., $U = U(y)$. Note that for the pipe $y^+ = \delta^+ - r^+$ such that this coordinate is zero at the wall. For these flows we also note that

$$-\frac{1}{\rho}\frac{\partial}{\partial x_i}\left(U_iP\right) = U\left(-\frac{1}{\rho}\frac{\partial P}{\partial x}\right), \tag{2}$$

and that the relation between the mean pressure gradient and the friction velocity is

$$-\frac{\delta}{\rho}\frac{\partial P}{\partial x} = u_\tau^2, \tag{3}$$

where $u_\tau = \sqrt{\tau_w/\rho}$. This gives

$$-\frac{1}{\rho}\frac{\partial}{\partial x_i}\left(U_iP\right) = \frac{u_\tau^2}{\delta}U. \tag{4}$$

Applying this and the noted assumptions yields

$$\frac{u_\tau^2}{\delta}U+\nu\frac{\partial^2}{\partial y^2}\left(\frac{1}{2}U^2\right)-\nu\frac{\partial U}{\partial y}\frac{\partial U}{\partial y}-U\frac{\partial\langle uv\rangle}{\partial y}=0. \tag{5}$$

The terms in Eq. (5) are now normalized using u_τ and ν. Following convention, this normalization is denoted by a superscript "+". Note that δ appears owing to (4).

Letting $T^+ = -\langle uv \rangle^+$, subsequent rearrangement yields the inner normalized equation for the mean kinetic energy in fully-developed turbulent channel flow

$$\frac{\partial^2}{\partial y^{+2}}\left(\frac{1}{2}U^{+2}\right)+U^+\frac{\partial T^+}{\partial y^+}-\frac{\partial U^+}{\partial y^+}\frac{\partial U^+}{\partial y^+}+\frac{1}{\delta^+}U^+=0. \quad (6)$$

The four terms presented in Eq. (6) are physically referred to as mean viscous diffusion (MVD), rate of work by net Reynolds stress (WRS), mean dissipation (MD) and mean pressure diffusion (MPD).

2. Zero-pressure gradient turbulent boundary layer

Relative to the channel or pipe, the differences in developing the equation for the flat plate boundary layer are associated with mean streamwise advection and a zero mean pressure gradient. Considering these, along with the boundary layer approximations, yields

$$U_k\frac{\partial}{\partial x_k}\left(\frac{1}{2}U_iU_i\right)=U\frac{\partial}{\partial x}\left(\frac{1}{2}U^2\right)+V\frac{\partial}{\partial y}\left(\frac{1}{2}U^2\right), \quad (7)$$

$$-\frac{1}{\rho}\frac{\partial}{\partial x_i}\left(U_iP\right)=0. \quad (8)$$

The other terms are the same as in channel/pipe flow. To within the boundary layer approximations, the inner-normalized equation for the mean kinetic energy in the zero-pressure gradient turbulent boundary layer is thus given by

$$\frac{\partial^2}{\partial y^{+2}}\left(\frac{1}{2}U^{+2}\right)+U^+\frac{\partial T^+}{\partial y^+}-\frac{\partial U^+}{\partial y^+}\frac{\partial U^+}{\partial y^+}+ \left[-U^+\frac{\partial}{\partial x^+}\left(\frac{1}{2}U^{+2}\right)-V^+\frac{\partial}{\partial y^+}\left(\frac{1}{2}U^{+2}\right)\right]=0. \quad (9)$$

The four physical terms in Eq. (9) are respectively denoted as mean viscous diffusion (MVD), rate of work by net Reynolds stress (WRS), mean dissipation (MD) and mean advection (MA).

3. Balance in mean kinetic energy budgets

As described in the Introduction, the mean momentum equation has a four-layer structure that is revealed by considering the ratio of the viscous force term, $VF = \partial^2 U^+/\partial y^{+2}$, to the turbulent inertia term, $TI = -\partial \langle u^+v^+\rangle/\partial y^+$, as a function of wall-normal position. The same methodology is now utilized to explore the leading order terms in Eqs. (6) and (9). In this case we consider the ratio of the sum of the mean viscous diffusion and mean dissipation terms ($MVD + MD$) to the rate of work by net Reynolds stress term (WRS). This ratio profile is shown in Figs. 2(a),(b) for channels and boundary layers, respectively.

Here we note that these profiles are identical to those of VF/TI. This observation is analytically verified by noting that the MVD term can be written as

$$\frac{\partial^2}{\partial y^{+2}}\left(\frac{1}{2}U^{+2}\right)=U^+\frac{\partial^2 U^+}{\partial y^{+2}}+\frac{\partial U^+}{\partial y^+}\frac{\partial U^+}{\partial y^+}, \quad (10)$$

which allows the mean kinetic energy equation to be written as

$$U^+\left(\frac{\partial^2 U^+}{\partial y^{+2}}+\frac{\partial T^+}{\partial y^+}+\frac{1}{\delta^+}\right)=0. \quad (11)$$

This relation also holds for the pipe, since the mean momentum equation for the pipe and channel can be written in identical forms. Similarly, the analogous construction holds for the boundary layer. The mean kinetic energy transport equation is therefore seen to exhibit the same layer structure as the mean momentum equation.

B. Total kinetic energy budgets

The turbulence kinetic energy equations are obtained through the same set of simplifications just employed, and for completeness their development is given in Appendix A. Here we now present the budgets for the total kinetic energy.

The combination of Eq. (6) and Eq. (A4) gives rise to the normalized budget equation for the total kinetic energy in channel flow (and pipe flow if the coordinate $y^+ = \delta^+ - r^+$ is employed)

$$\frac{\partial^2}{\partial y^{+2}}\left(\frac{1}{2}U^{+2}+K^+\right)+\frac{\partial}{\partial y^+}\left[U^+T^+-\langle v^+K^+\rangle\right] +D^+ +\frac{1}{\delta^+}\left[U^+-\frac{\partial}{\partial y^+}\langle p^+v^+\rangle\right]=0, \quad (12)$$

where $D^+ = -\left[d^+ + (\partial U^+/\partial y^+)^2\right]$. Four physical mechanisms are present in Eq. (12). These are viscous diffusion (VD), production/turbulent diffusion (PT), dissipation (D) and total pressure diffusion (PD).

The combination of Eq. (9) and Eq. (A7) gives rise to the normalized budget equation for the total kinetic energy in the boundary layer,

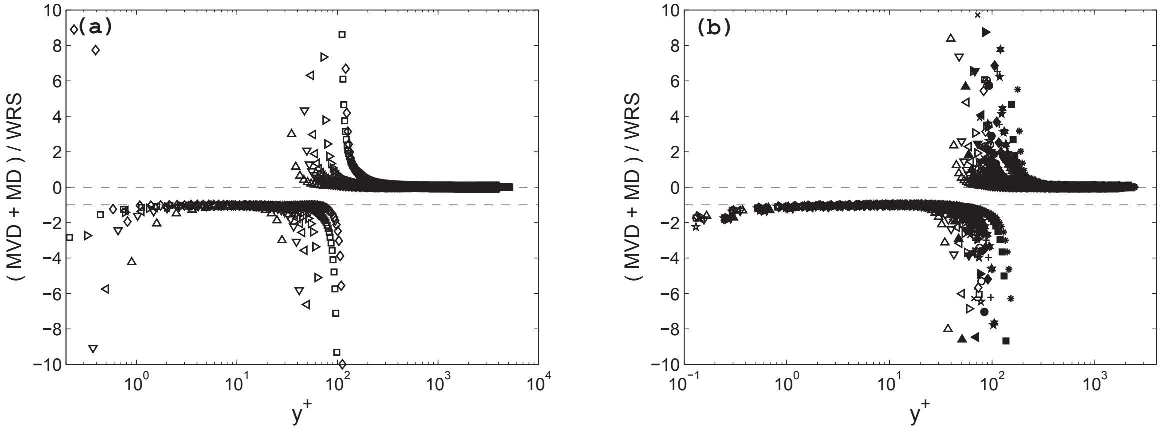

FIG. 2. Ratio of the sum of mean viscous diffusion and mean dissipation terms ($MVD + MD$) to the rate of work by net Reynolds stress term (WRS). (a) Fully developed channel flows, DNS data are from Hoyas *et al.* [28] :$\triangle, \delta^+ = 186$; $\triangledown, \delta^+ = 547$; $\triangleleft, \delta^+ = 934$; $\triangleright, \delta^+ = 2003$; Bernardini *et al* [29] : $\Diamond, \delta^+ = 4079$; Lee & Moser[30] : $\square, \delta^+ = 5186$. (b) Zero pressure gradient turbulent boundary layers, DNS and LES data are from Eitel-Amor *et al.*.[31] : $\triangle, \delta^+ = 252$; $\triangledown, \delta^+ = 359$; $\blacktriangle, \delta^+ = 458$; $\triangleleft, \delta^+ = 492$; $\triangleright, \delta^+ = 671$; $\blacktriangledown, \delta^+ = 725$; $\times, \delta^+ = 830$; $\blacktriangleleft, \delta^+ = 957$; $\cdot, \delta^+ = 974$; $\Diamond, \delta^+ = 1043$; $\circ, \delta^+ = 1145$; $\blacktriangleright, \delta^+ = 1169$; $\square, \delta^+ = 1244$; ☆, $\delta^+ = 1271$; $\bullet, \delta^+ = 1367$; $+, \delta^+ = 1561$; ♦, $\delta^+ = 1751$; ✸, $\delta^+ = 1937$; $\blacksquare, \delta^+ = 2118$; ★, $\delta^+ = 2299$; ✳, $\delta^+ = 2479$.

$$\frac{\partial^2}{\partial y^{+2}}\left(\frac{1}{2}U^{+2} + K^+\right) + \frac{\partial}{\partial y^+}\left[U^+T^+ - \left\langle v^+K^+\right\rangle\right] + D^+ +$$
$$\left[-U^+\frac{\partial}{\partial x^+}\left(\frac{1}{2}U^{+2} + K^+\right) - V^+\frac{\partial}{\partial y^+}\left(\frac{1}{2}U^{+2} + K^+\right) - \frac{1}{\delta^+}\frac{\partial}{\partial y^+}\left\langle p^+v^+\right\rangle\right] = 0. \tag{13}$$

The different terms of Eq. (13) are referred to as viscous diffusion (VD), production/turbulent diffusion (PT), dissipation (D) and advection/turbulent pressure diffusion (APD).

C. Terms in the total kinetic energy budgets

Analysis begins by individually considering the behaviors of the four grouped terms in Eqs. (12) and (13). Figs. 3 (a)-(l) show profiles of the terms. The first three terms for the channel, pipe, and boundary layer exhibit nearly the same behavior. The profiles of the VD and D terms convincingly merge for all Reynolds numbers plotted, except immediately adjacent to the wall in the channel and pipe. Here the VD term appears to consistently increase with Reynolds number below $y^+ \simeq 3$, and the D term decreases with Reynolds number below $y^+ \simeq 7$. Hoyas *et al.* [28] attribute these behaviors to the effect of the large scale inactive motions that exist in the logarithmic layer. Existing evidence indicates that this is a weak but persistent Reynolds number dependence [3]. The VD term has a value of about 1.2 close to the wall. Starting near $y^+ = 2$ this profile decreases rapidly and crosses zero at $y^+ \simeq 7.5$ and 7.75 in the channel and pipe, respectively, and at $y^+ \simeq 7.3$ for the boundary layer. The VD profiles reach their minimum values near $y^+ = 15$, but increase thereafter to approach zero from below. Opposite to the VD term, the D term begins at a value of about -1.2 close to the wall but increases more gradually as it approaches zero from below. The VD and D terms identically balance at the wall.

The PT term profiles in Figs. 3 start with a zero value at the wall, and rapidly ascend. The peaks in all the profiles attain values of about 0.70 near $y^+ = 9.0$. Beyond the peak, the PT term descends to cross zero from positive to negative. The negative portion of this profile is concave-upward, and this characteristic is more evident for the boundary layer. The position of the zero-crossing in the PT term moves to greater y^+ values with increasing δ^+.

The PD and APD terms in Figs. 3 (g) and (h) are both zero at the wall, and become larger with increasing distance from the wall. The maximum values of these profiles are Reynolds number dependent. Moreover, there is an obvious peak in the APD profile, and this term decreases towards zero in the outer region. This is qualitatively distinct from the PD profiles in the pipe and channel, which exhibit highly similar profile shapes, but small quantitative differences. In the overall balance, the behavior of the APD profile has been verified to compensate for the concave-upward trend of the PT term near the edge of the boundary layer. In the region near the wall, the PD term in the pipe and channel and the APD

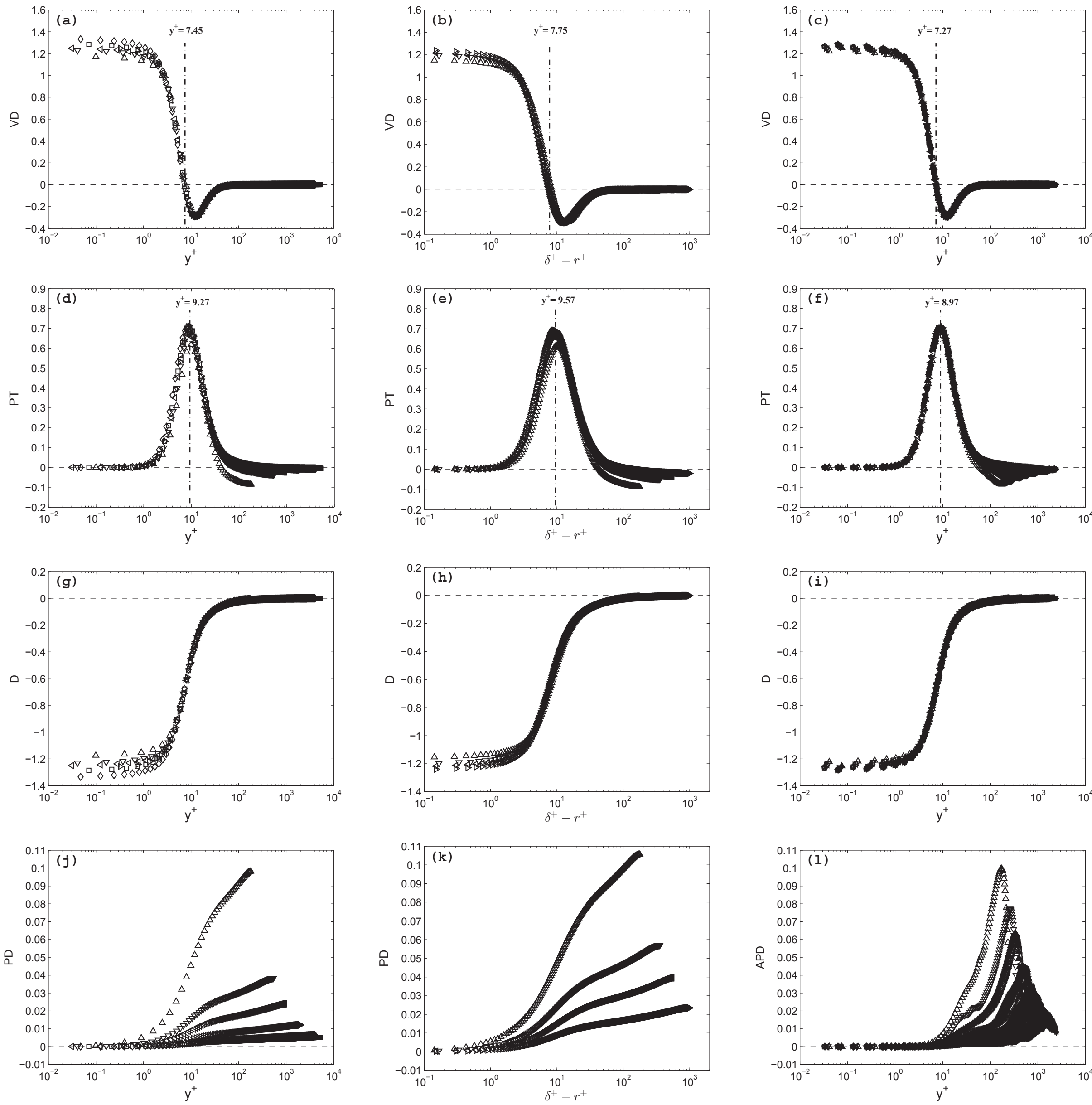

FIG. 3. Profiles of the individual terms in the total kinetic energy transport equation. Panels (a), (d), (g) and (j) respectively represent the VD, PT, D, and PD terms for turbulent channel flow, (b), (e), (h), (k) respectively represent the VD, PT, D, and PD terms for turbulent pipe flows, and (c), (f), (i) and (l) respectively represent the VD, PT, D and APD terms for turbulent boundary layer flows. The vertical dashed-dotted line in (a) - (c) denotes the wall-normal position where the VD crosses zero from positive to negative. The vertical dashed-dotted line in (d) - (f) denotes the wall-normal position where the PTD achieves its maximal value. The pipe flow data are from the DNS of [32].

term in the boundary layer are much smaller than the other three terms, but both rise to leading order in the outer region.

III. STRUCTURE OF TOTAL KINETIC ENERGY BALANCE

A. Balance ratios of grouped terms

The analysis of section II A 3 reveals a mean kinetic energy layer structure that is the same as for the mean momentum balance (see of Fig. 2). This finding motivates examining the analogous ratio in the total kinetic

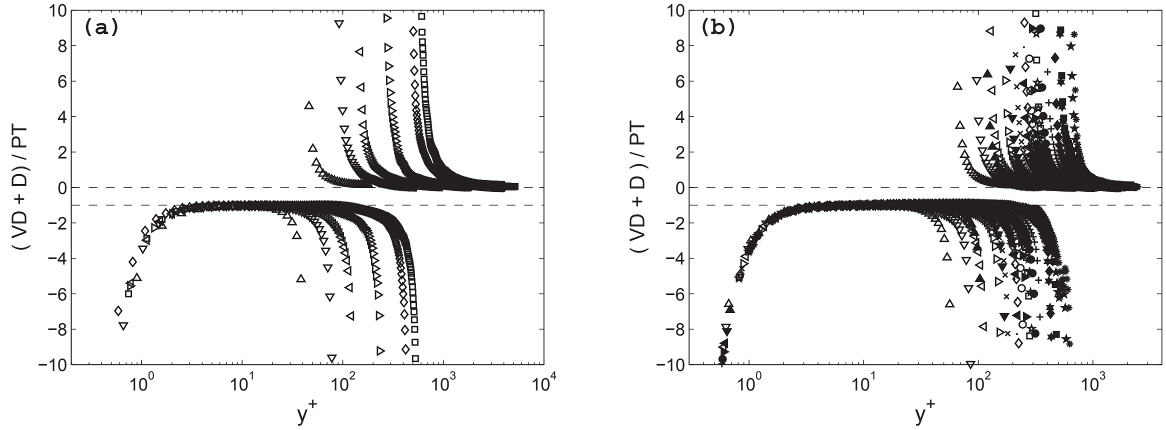

FIG. 4. Ratio of the sum of the viscous diffusion (VD) and the dissipation (D) terms to the production/turbulent diffusion (PT) term versus y^+. (a) Channel flows. (b) Boundary layer flows. Symbols are the same as in Fig. 2.

energy equation: the ratio of the sum of the viscous diffusion and the dissipation terms ($VD + D$) to the production/turbulent diffusion term (PT). Here we note that if the ratio is

$$|(VD + D) / PT| \ll 1, \tag{14}$$

then both the VD and D terms are small, and the PT and the PD terms are nominally in balance. If

$$|(VD + D) / PT| \cong 1, \tag{15}$$

their effects are in balance, and the PD term is either of the same order of magnitude or much smaller. Else, if

$$|(VD + D) / PT| \gg 1, \tag{16}$$

the PT term is very small, and either the VD term is balanced with the D term or the PD term is of the same order of magnitude as these two terms.

Figs. 4 (a) and (b) show $(VD + D) / PT$ for the channel and boundary layer, respectively, with the pipe data (not shown) exhibiting similar behaviors. These data indicate a four-layer structure. This structure is, however, distinct from the layer structure identified by Wei *et al.* [20] for the mean momentum equation, which, as shown herein, also corresponds with the mean kinetic energy structure. To avoid confusion with the layers associated with the mean momentum equation, in what follows the layers evident in Figs. 4 are denoted with lower case i-iv. The analysis now proceeds by describing how the contributing terms in Eqs. (12) and (13) conspire to produce the layer structure evident in Figs. 4.

B. Layers i and ii

Layer i lies very close to the wall, $y^+ \lesssim 1.5$. The ending value cited is based on the criterion that the ratio becomes less than -2 [20]. In this domain, the leading balance is between the viscous diffusion and dissipation term, as exemplified in Fig. 5 for the channel and boundary layer. Here the ratio VD/D deviates from -1 by less than 4%. Outside this thin layer exists a region (layer ii) that is characterized by a nearly exact balance between the sum of the VD and D terms and the PT term. At the onset of this region the viscous diffusion term is positive, but with increasing y^+ goes to zero faster than the dissipation term. It subsequently crosses zero, reaches a minimum, and then asymptotes to zero. Beyond where the VD term crosses zero, its magnitude contribution to the sum of the VD and D terms increases gradually and attains a maximum, see Figs. 3 and 5. This maximum is slightly greater than half the contribution to the sum (about 54%), and is located near $y^+ \simeq 18$.

For greater distances from the wall, but still within layer ii, the contribution from the VD term decreases and becomes negligible compared to the D term. This occurs near the outer edge of layer ii. Fig. 3 shows that near the start of layer ii, the PT term increases to balance the VD and D terms; achieving peak values of about 0.70 near $y^+ = 9.0$. The extent of layer ii exhibits a Reynolds number dependence, with its external boundary extending into the inertial/advection balance layer (layer IV) of the mean momentum equation.

C. External bounds of layers ii and iii

Per the criterion developed by Wei *et al* [20], the start of layer iii is where $(VD + D) / PT$ drops below -2. Consistently, the end of layer iii is where this ratio falls below 0.5. Fig. 6 shows the normalized width of layer iii (Δy^+_{iii}) versus δ^+ for channel, pipe, and, boundary layer flows as determined by these criteria. Per the scaling analysis of Appendix C, Δy^+_{iii} is normalized by $(\delta^+ - \sqrt{\delta^+})$, as this is reasoned to constitute a finite Reynolds number correction to outer normalization. To within their scatter, the

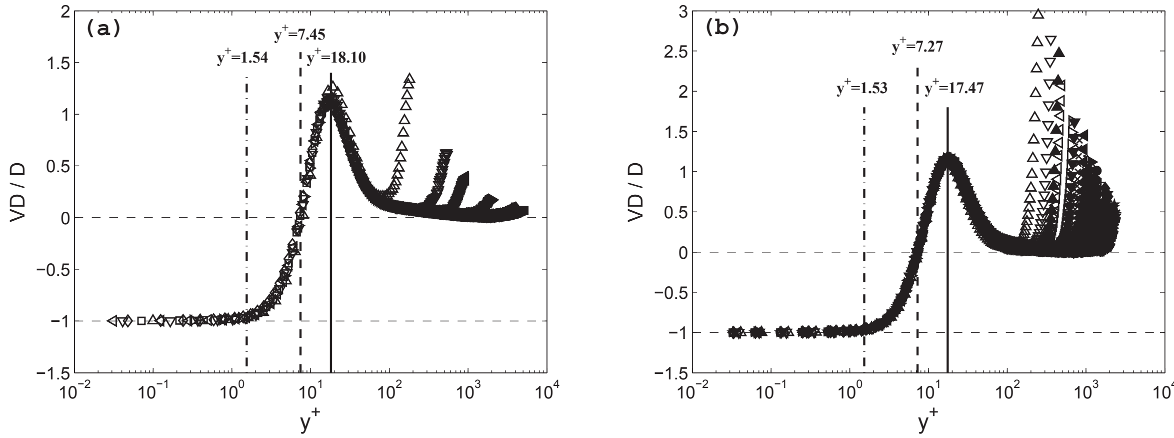

FIG. 5. Ratio of viscous diffusion (VD) to dissipation (D). (a) Channel flows; (b) Boundary layers. The vertical dashed-dotted line denotes the external bound of layer I. The vertical dashed line denotes the position where the viscous diffusion crosses zero. The vertical solid line denotes the position where the ratio peaks. Symbols are the same as in Fig. 2.

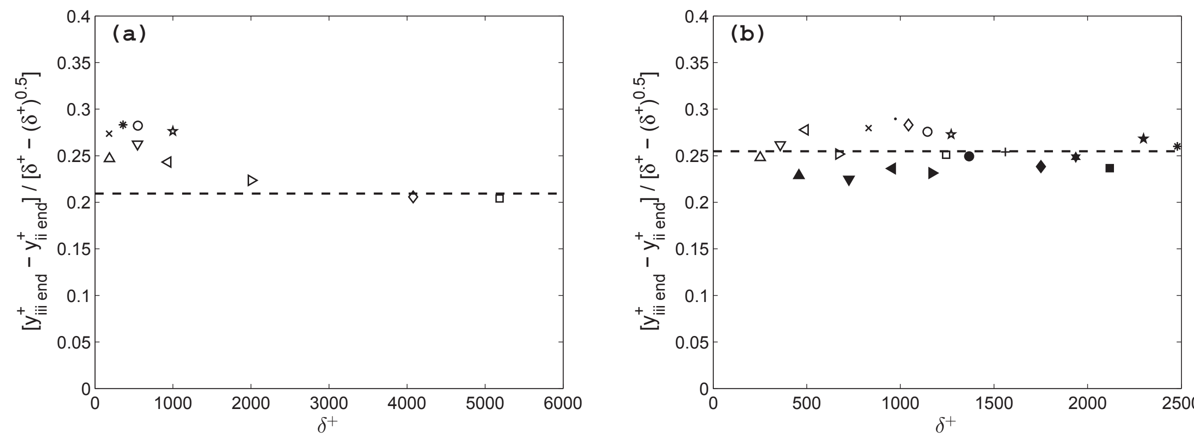

FIG. 6. Width of layer iii normalized by $(\delta^+ - \sqrt{\delta^+})$ and plotted versus δ^+. (a) Channel and pipe flows. channel: $\triangle, \delta^+ = 186$; $\bigtriangledown, \delta^+ = 547$; $\triangleleft, \delta^+ = 934$; $\triangleright, \delta^+ = 2003$; $\Diamond, \delta^+ = 4079$; $\square, \delta^+ = 5186$. Pipe: $\times, \delta^+ = 181$; $\ast$, $\delta^+ = 361$; $\circ, \delta^+ = 550$; $\star$, $\delta^+ = 999$. Horizontal line is at 0.2093. (b) Boundary layer flows: $\triangle, \delta^+ = 252$; $\bigtriangledown, \delta^+ = 359$; $\blacktriangle, \delta^+ = 458$; $\triangleleft, \delta^+ = 492$; $\triangleright, \delta^+ = 671$; $\blacktriangledown, \delta^+ = 725$; $\times, \delta^+ = 830$; $\blacktriangleleft, \delta^+ = 957$; $\cdot, \delta^+ = 974$; $\Diamond, \delta^+ = 1043$; $\circ, \delta^+ = 1145$; $\blacktriangleright, \delta^+ = 1169$; $\square, \delta^+ = 1244$; $\star$, $\delta^+ = 1271$; $\bullet, \delta^+ = 1367$; $+, \delta^+ = 1561$; $\blacklozenge, \delta^+ = 1751$; ✶, $\delta^+ = 1937$;$\blacksquare, \delta^+ = 2118$; $\bigstar, \delta^+ = 2299$; $\ast$, $\delta^+ = 2479$. Horizontal line is at 0.2549.

boundary layer data of Fig. 6 seem to remain constant over their entire Reynolds number range. Conversely, the channel data seem to decay toward a constant value with increasing δ^+. The pipe flow data show a similar trend as the channel data, but only extend to $\delta^+ \simeq 1000$.

While the analysis of Appendix C indicates that Δy^+_{iii} should scale with $(\delta^+ - \sqrt{\delta^+})$ at finite δ^+, this analysis does not require that the beginning and end points of layer iii individually adhere to this scaling. This rather subtle point is clarified in Fig. 7, which re-plots the data of Fig. 4 versus $y^+/(\delta^+ - \sqrt{\delta^+})$. The data of Fig. 7(b) suggest invariance under this normalization, and thus the end points of layers ii and iii in the boundary layer seem to scale with $(\delta^+ - \sqrt{\delta^+})$. On the other hand, examination of the channel and pipe data reveals that the end points of both layers ii and iii deviate from this scaling over the given δ^+ range. As exemplified in Fig. 7(a), the channel data at $\delta^+ = 186$ show a considerable deviation from those at higher δ^+. With increasing δ^+, however, the profile-to-profile deviation diminishes. The deviation of the $\delta^+ = 186$ profile in Fig. 7(a) is not especially surprising, since this profile is just barely within regime where the mean momentum equation exhibits its four layer structure [33]. Additionally, it has been verified that both the channel and pipe profiles exhibit the same qualitative behavior when plotted versus y/δ. Determining whether the beginning and end points of layer iii for the channel and pipe eventually align under the normalization of Fig. 7 awaits higher Reynolds number data.

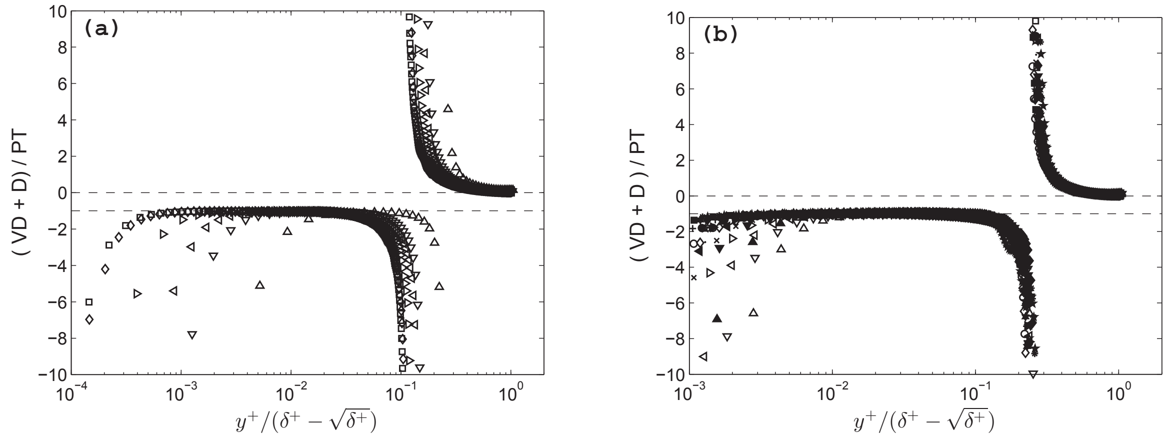

FIG. 7. Profiles of Fig. 4 plotted versus $y^+/(\delta^+ - \sqrt{\delta^+})$. (a) Channel flows. (b) Boundary layer flows. Symbols are the same as in Fig. 2.

D. Layers iii and iv

Across layer iii there is an exchange in the balance of terms in Eqs. (12) and (13) that we now describe but do not graphically demonstrate. This exchange occurs around the location of maximum $[U^+T^+ - \langle v^+K^+\rangle]$. In this region the dissipation (D) term and the total pressure diffusion (PD) term in channel/pipe flows (or the advection/turbulent pressure diffusion (APD) term in boundary layers) nearly balance. Before and beyond the peak in $[U^+T^+ - \langle v^+K^+\rangle]$, the PT term is in leading order balance with the sum of the D and PD terms in channel and pipe flows, and balances the $D+APD$ terms in boundary layers. The VD term in this layer is less than a tenth of the D term. Thus, within layer iii, there are three terms of significant magnitude, with the VD term being much smaller.

Close examination also indicates that across layer iii the PT term changes its sign, and the contribution from turbulent diffusion is much smaller when compared to the contribution from the production term. This characteristic is reflected in the results of Fig. 8. Accordingly, the wall-normal position where the production term crosses zero is very close to where the PT term crosses zero. These findings substantiate that the turbulent diffusion term over layer iii is quite small. We therefore surmise that the turbulent diffusion term is small but non-negligible in layer ii, but attains negligible values in layer iii.

The dissipation term is dominated by its turbulence contribution in layer iii. This is demonstrated in Figs. 9(a) and (b), which show the ratios of the mean to turbulent dissipation. In these figures, the abscissa starts near the outer edge of layer ii at $\delta^+ = 180$ and 252 for the turbulent channels and boundary layers, respectively. Beyond the start of layer iii the mean dissipation is at least 10 times smaller than the turbulent dissipation, and its effect over layer iii diminishes with increasing δ^+. These findings are similar to previous observations that the fluctuating enstrophy dominates the mean enstrophy in layer IV of the mean momentum equation [21].

The ratio of the turbulent pressure diffusion to the mean pressure diffusion is exemplified for the channel in Fig. 10(a), while the ratio of turbulent pressure diffusion to advection in the boundary layer is given in Fig. 10(b). The fact that these ratios are both less than 10^{-3} beyond layer ii indicates that the turbulent pressure diffusion is justifiably absent from the leading balance in layer iii. The layer iii balance in the channel/pipe therefore simplifies to

$$\frac{\partial}{\partial y^+}\left[U^+T^+\right] + d^+ + \epsilon^2 U^+ = 0, \tag{17}$$

where $\epsilon^2 = 1/\delta^+$, and for the boundary layer is

$$\frac{\partial}{\partial y^+}\left[U^+T^+\right] + d^+ + \left[-U^+\frac{\partial}{\partial x^+}\left(\frac{1}{2}U^{+2} + K^+\right) - V^+\frac{\partial}{\partial y^+}\left(\frac{1}{2}U^{+2} + K^+\right)\right] = 0. \tag{18}$$

Beyond layer iii, the magnitude of both the VD and D terms gradually become smaller than either the PT or PD terms in the channel/pipe flows, or the APD term in the boundary layer. Similarly, both the turbulent diffusion and the turbulent pressure diffusion are much smaller than their mean contributions. Thus, the balance

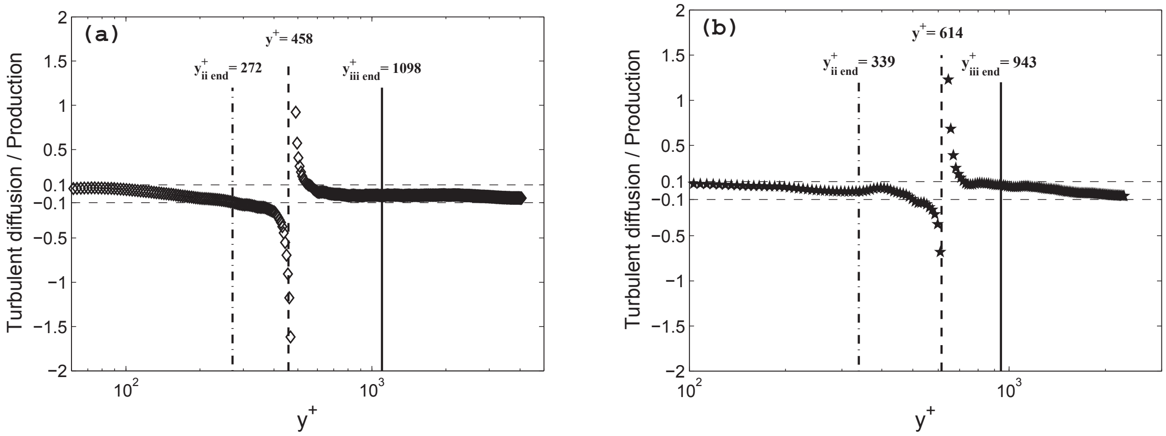

FIG. 8. Ratio of turbulent diffusion to production. (a) Channel flow at $\delta^+ = 4079$; (b) Boundary layer at $\delta^+ = 2299$. The vertical dashed-dotted line denotes the external bound of layer ii. The vertical dashed line denotes where the (PT) term crosses zero. The vertical solid line denotes the external bound of layer iii.

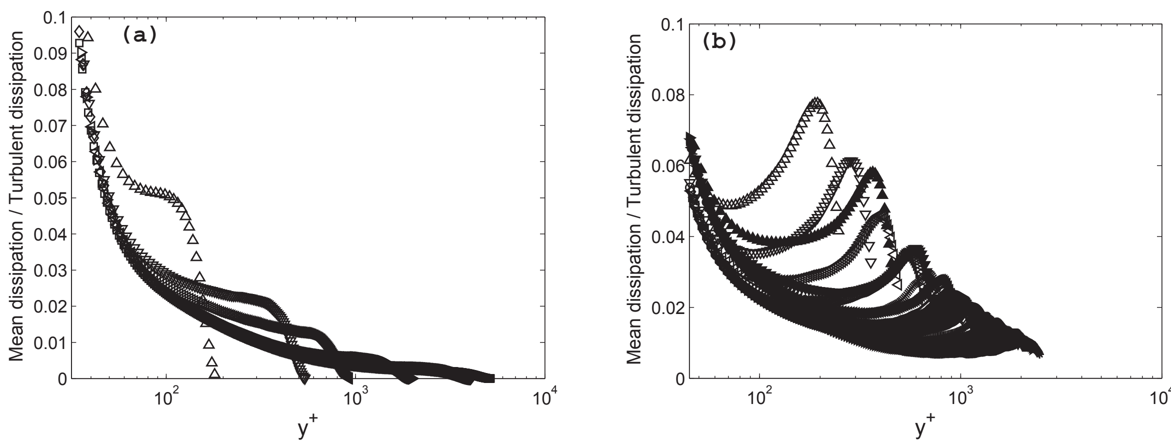

FIG. 9. The ratio of the mean dissipation to the turbulent dissipation. (a) Turbulent channel flows; (b) Turbulent boundary layers.

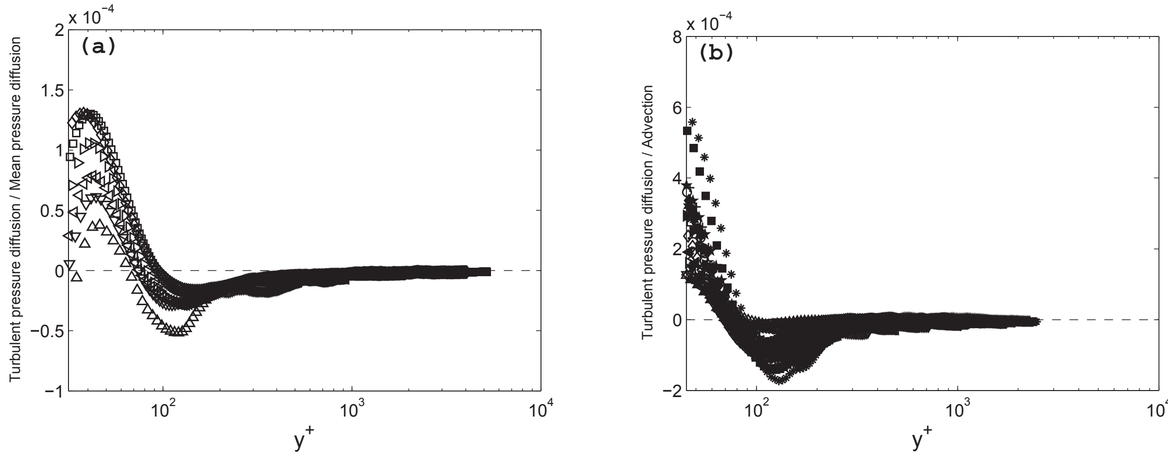

FIG. 10. (a) Ratio of turbulent pressure diffusion to mean pressure diffusion in channel flows; (b) Ratio of turbulent pressure diffusion to advection in boundary layers.

is established between the production and mean pressure diffusion for channel/pipe flows

$$\frac{\partial}{\partial y^+}\left[U^+T^+\right] + \frac{1}{\delta^+}U^+ = 0, \tag{19}$$

and between the production and the advection for boundary layers, i.e.,

$$\frac{\partial}{\partial y^+}\left[U^+T^+\right] + \left[-U^+\frac{\partial}{\partial x^+}\left(\frac{1}{2}U^{+2}+K^+\right) - V^+\frac{\partial}{\partial y^+}\left(\frac{1}{2}U^{+2}+K^+\right)\right] = 0. \tag{20}$$

Eqs. (17) and (19) respectively give the leading balances in layers iii and iv for the channels and pipes, and Eqs. (18) and (20) give the same for the boundary layer.

Since

$$\frac{\partial\left(U^+T^+\right)}{\partial y^+} = U^+\left(\frac{\partial T^+}{\partial y^+}\right) + T^+\left(\frac{\partial U^+}{\partial y^+}\right), \tag{21}$$

the individual behaviors of the two contributions on the right are of interest. Figs. 11 (a) and (b) respectively show profiles of the terms in Eqs. (17) and (18) across layers iii and iv. These representative profiles are shown at a single δ^+ for the channel and boundary layer. Within layer iii, the four relevant terms are of the same order of magnitude but have different trends. The turbulent dissipation profile gradually moves towards zero from below and crosses the $U^+\left(\partial T^+/\partial y^+\right)$ profile, which passed through zero to negative values in layer ii. Above the zero axis, the $T^+\left(\partial U^+/\partial y^+\right)$ and $\epsilon^2 U^+$ profiles exhibit a similar crossing. These crossing points exhibit a Reynolds dependence that is consistent with its position residing within layer iii for all δ^+. The two crossing positions for channels and boundary layers are respectively plotted versus $(\delta^+ - \sqrt{\delta^+})$ in Figs. 12 (a) and (b), while it has been confirmed that the pipe exhibits behaviors very similar to those in the channel. These data indicate that the $T^+\left(\partial U^+/\partial y^+\right)$ and $\epsilon^2 U^+$ (or advection) terms cross slightly closer to wall than the $U^+\left(\partial T^+/\partial y^+\right)$ and d^+ terms at lower Reynolds numbers, but these positions essentially coincide at higher δ^+. Similar to the phenomena illustrated in Fig. 7, the channel data gradually approach the indicated curve-fit line with increasing Reynolds number, while the boundary layer data convincingly follow the linear curve-fit for all δ^+. For all three flows the profile-crossings occur slightly closer to $y^+_{ii\ end}$ than $y^+_{iii\ end}$.

Both the $T^+\left(\partial U^+/\partial y^+\right)$ and the d^+ terms lose leading order in layer iv, becoming negligible compared to the $U^+\left(\partial T^+/\partial y^+\right)$ and $\epsilon^2 U^+$ terms, or similarly the advection term in the boundary layer. Figs. 13 (a) and (b) respectively show profiles of the ratio of $U^+\left(\partial T^+/\partial y^+\right)$ to $\epsilon^2 U^+$ (or advection term), and the ratio of $T^+\left(\partial U^+/\partial y^+\right)$ to d^+. As might be expected, although both the $T^+\left(\partial U^+/\partial y^+\right)$ and d^+ terms are much smaller than the other two terms (and thus are not leading order), their ratio is nearly -1. This ratio then approaches zero at the edge of layer iv. Beyond the outer edge of layer ii the traditional production term, $T^+\left(\partial U^+/\partial y^+\right)$, is initially balanced with the turbulent dissipation term, d^+, but with the traditional production term approaching zero more rapidly as $y^+ \to \delta^+$.

The ratio of the other two leading order terms is also approximately -1 throughout layer iv. This balance begins near the middle of layer iii for the channel/pipe, and near the outer edge of layer ii for the boundary layer. It is thus concluded that beyond layer ii, the $U^+\left(\partial T^+/\partial y^+\right)$ term balances with the $\epsilon^2 U^+$ term for the channel/pipe, and similarly with the advection term for the boundary layer. Notably, the two separate balances in Fig. 11 reflect the individual balances of the mean and turbulence kinetic energy equations.

IV. CONCLUSIONS AND DISCUSSION

Properties of the layer structure associated with the total kinetic energy equation are summarized in Table I. From this table, it is evident that channel, pipe, and boundary layer flows qualitatively exhibit the same behaviors to within the differences between the mean pressure and mean advection effects. Quantitatively, the layer thicknesses are shown herein to exhibit distinct Reynolds number dependencies. As is evident, layer i adheres to inner scaling. The analysis of Appendix C leads us to surmise that the layer iii width follows a $(\delta^+ - \sqrt{\delta^+})$ dependence at finite Reynolds numbers. This result appears to hold in the boundary layer for all observed δ^+, and also seems to hold for the individual upper boundaries of layers ii and iii. In the channel the present estimates suggest that the layer iii width scales with this length for $\delta^+ > 1000$. The layer scaling behaviors associated with the total kinetic energy differ substantially from those of the mean momentum balance. It is significant to note, however, that the layer structure of the mean kinetic energy equation, which is identical to that of the mean momentum equation, is embedded within this structure.

The present results indicate that the major portions of layers ii and all of layer iii and iv reside in the inertial/advection balance layer (layer IV) of the mean momentum balance. Here the Reynolds stress gradient balances the pressure force in channel flow or the mean ad-

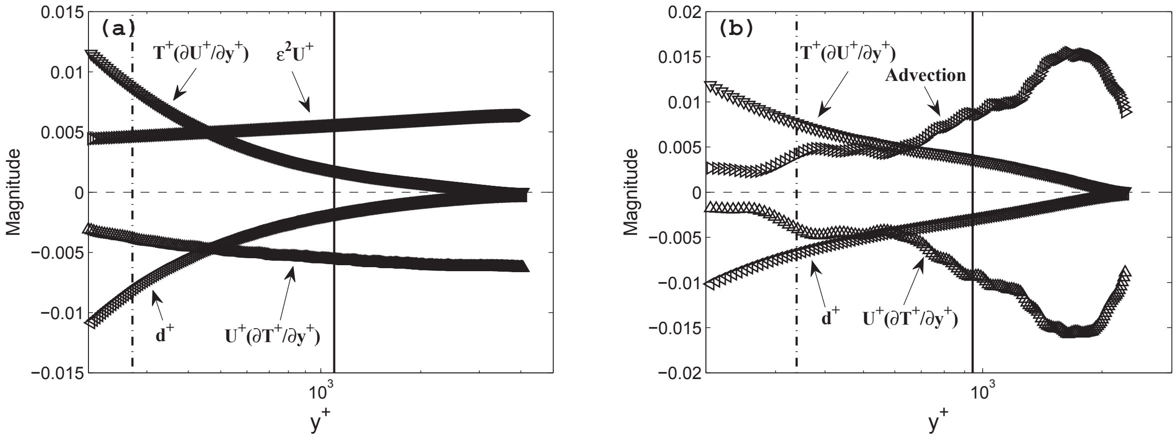

FIG. 11. (a) Profiles of terms in Eq. (17) across layer iii and iv at $\delta^+ = 4079$. $\triangle, U^+\left(\partial T^+/\partial y^+\right)$; $\bigtriangledown, T^+\left(\partial U^+/\partial y^+\right)$; $\triangleleft$, turbulent dissipation d^+; $\triangleright, \epsilon^2 U^+$; (b) Profiles of terms in Eq. (18) across layer iii and iv at $\delta^+ = 2299$. $\triangle, U^+\left(\partial T^+/\partial y^+\right)$; $\bigtriangledown, T^+\left(\partial U^+/\partial y^+\right)$; $\triangleleft$, turbulent dissipation d^+; $\triangleright$, advection. The vertical dashed-dotted line denotes the external bound of layer ii. The vertical solid line denotes the external bound of layer iii.

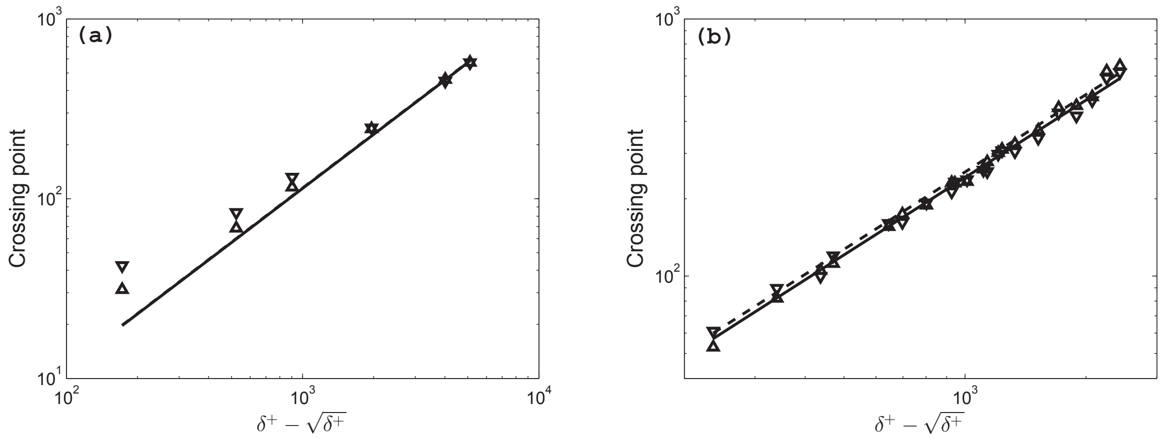

FIG. 12. Reynolds number dependence of the two crossing points in Fig. 11. (a) Channel flows. $\triangle$, crossing point between $T^+\left(\partial U^+/\partial y^+\right)$ and $\epsilon^2 U^+$, curve fit is given by dashed line which is $0.1145(\delta^+ - \sqrt{\delta^+})$; $\bigtriangledown$, crossing point between $U^+\left(\partial T^+/\partial y^+\right)$ and turbulent dissipation d^+, curve fit is given by solid line which is $0.1140(\delta^+ - \sqrt{\delta^+})$. (b) Boundary layers. $\triangle$, crossing point between $T^+\left(\partial U^+/\partial y^+\right)$ and advection term, curve fit is given by dashed line which is $0.2542(\delta^+ - \sqrt{\delta^+})$; $\bigtriangledown$, crossing point between $U^+\left(\partial T^+/\partial y^+\right)$ and turbulent dissipation d^+, curve fit is given by solid line which is $0.2419(\delta^+ - \sqrt{\delta^+})$.

TABLE I. Magnitude ordering and approximate scaling behaviors associated with the four layer structure of the total kinetic energy equations for channel/pipe and boundary layer. VD, D, PT, PD and APD respectively refer to the viscous diffusion, dissipation, production/turbulent diffusion, total pressure diffusion and advection/turbulent pressure diffusion terms in Eqs. (12) and (13). Note that $\left(\delta - \sqrt{\nu\delta/u_\tau}\right)$ approaches δ as $\delta^+ \to \infty$.

	Channel/Pipe flow		Boundary layer flow	
Layer	Magnitude ordering	Δy increment	Magnitude ordering	Δy increment
i	$\lvert VD\rvert \cong \lvert D\rvert$	$O\left(\nu/u_\tau\right)(\cong 1.5)$	$\lvert VD\rvert \cong \lvert D\rvert$	$O\left(\nu/u_\tau\right)(\cong 1.5)$
ii	$\lvert VD\rvert \cong \lvert D\rvert \cong \lvert PT\rvert$	$O\left(\delta - \sqrt{\nu\delta/u_\tau}\right)(\cong 0.07)$	$\lvert VD\rvert \cong \lvert D\rvert \cong \lvert PT\rvert$	$O\left(\delta - \sqrt{\nu\delta/u_\tau}\right)(\cong 0.17)$
iii	$\lvert D\rvert \cong \lvert PT\rvert \cong \lvert PD\rvert$	$O\left(\delta - \sqrt{\nu\delta/u_\tau}\right)(\cong 0.21)$	$\lvert D\rvert \cong \lvert PT\rvert \cong \lvert APD\rvert$	$O\left(\delta - \sqrt{\nu\delta/u_\tau}\right)(\cong 0.25)$
iv	$\lvert PT\rvert \cong \lvert PD\rvert$	$O(\delta)(\cong 0.68)$	$\lvert PT\rvert \cong \lvert APD\rvert$	$O(\delta)(\cong 0.58)$

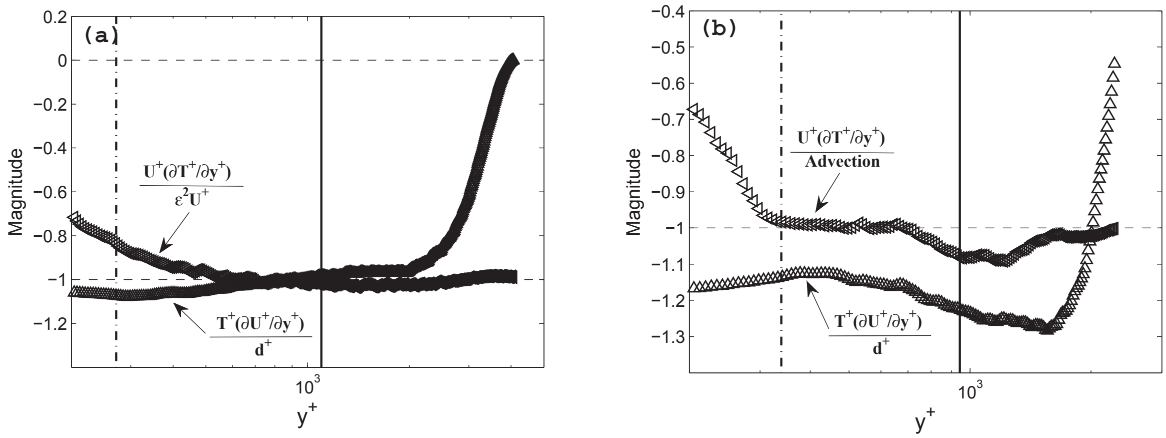

FIG. 13. (a)Ratios of ($\triangleleft$) $U^+\left(\partial T^+/\partial y^+\right)$ to $\epsilon^2 U^+$ and ($\triangle$) $T^+\left(\partial U^+/\partial y^+\right)$ to turbulent dissipation d^+ for turbulent channel flow at $\delta^+ = 4079$. (b) Ratios of ($\triangleleft$) $U^+\left(\partial T^+/\partial y^+\right)$ to advection term and ($\triangle$) $T^+\left(\partial U^+/\partial y^+\right)$ to turbulent dissipation d^+ for turbulent boundary layer at $\delta^+ = 2299$.

vection in the boundary layer flow, while the viscous force is negligible. For the total kinetic energy balance the viscous diffusion term gradually becomes negligible near the external bound of layer ii, and the dissipation term loses leading order in layer iv. The leading order balance is inviscid in the outer 30% of the channel/pipe, and outer 40% of the boundary layer.

Lastly, we note that the leading order balances associated with the total kinetic energy budget exhibit an intriguing and potentially telling set of behaviors. Recalling that the total budget is the sum of the mean and turbulence budgets, the relevant behaviors are that mean budget contributions dominate the leading terms near the wall, the turbulence equation contributions become leading order over an interior region, and then in the outermost portion mean equation terms return to dominance. This spatial inter-weaving of the leading order contributions suggests that care should be taken when using traditional Reynolds averaging to discern properties associated with the energetic motions within the flow.

ACKNOWLEDGMENTS

This work was supported by the National Science Foundation and the Australian Research Council. The present authors express their gratitude to the researchers cited herein who made their DNS data publicly available.

Appendix A: Turbulence kinetic energy budgets

1. Channel flow

Beginning with the general budget equation for the kinetic energy of the turbulence,

$$\frac{\partial}{\partial t}\left[\frac{1}{2}\langle u_i u_i\rangle\right] + U_k\frac{\partial}{\partial x_k}\left[\frac{1}{2}\langle u_i u_i\rangle\right] = -\frac{\partial}{\partial x_k}\left[\left\langle u_k\frac{1}{2}u_i u_i\right\rangle + \frac{1}{\rho}\langle u_k p\rangle\right] + \nu\frac{\partial^2}{\partial x_k\partial x_k}\left[\frac{1}{2}\langle u_i u_i\rangle\right] - \langle u_i u_k\rangle\frac{\partial U_i}{\partial x_k} - \nu\left\langle\frac{\partial u_i}{\partial x_k}\frac{\partial u_i}{\partial x_k}\right\rangle, \tag{A1}$$

and applying the same assumptions noted in section II, one arrives at the budget equation for the turbulence kinetic energy in fully-developed channel flow

$$-\frac{\partial}{\partial y}\left\langle v\frac{1}{2}u_i u_i\right\rangle - \frac{\partial}{\partial y}\frac{1}{\rho}\langle vp\rangle + \nu\frac{\partial^2}{\partial y^2}\left[\frac{1}{2}\langle u_i u_i\rangle\right] - \langle uv\rangle\frac{\partial U}{\partial y} + d = 0, \tag{A2}$$

where $d = -\nu\left\langle\frac{\partial u_i}{\partial x_k}\frac{\partial u_i}{\partial x_k}\right\rangle$. All terms in Eq. (A2) are now normalized by inner variables, but with

$$p^+ = \frac{\delta p}{\rho u_\tau \nu}. \tag{A3}$$

Here, the pressure fluctuation is normalized with $\rho u_\tau \nu/\delta$ rather than by ρu_τ^2. This follows from the analogous scaling of the mean pressure gradient in terms of the friction velocity and the half-channel height (Eq. (4)). Physically, this seems appropriate because the fluctuating pressure is a non-local quantity, with the pressure at a point found by integrating over the domain. The analysis of Appendix B empirically evidences that the use of

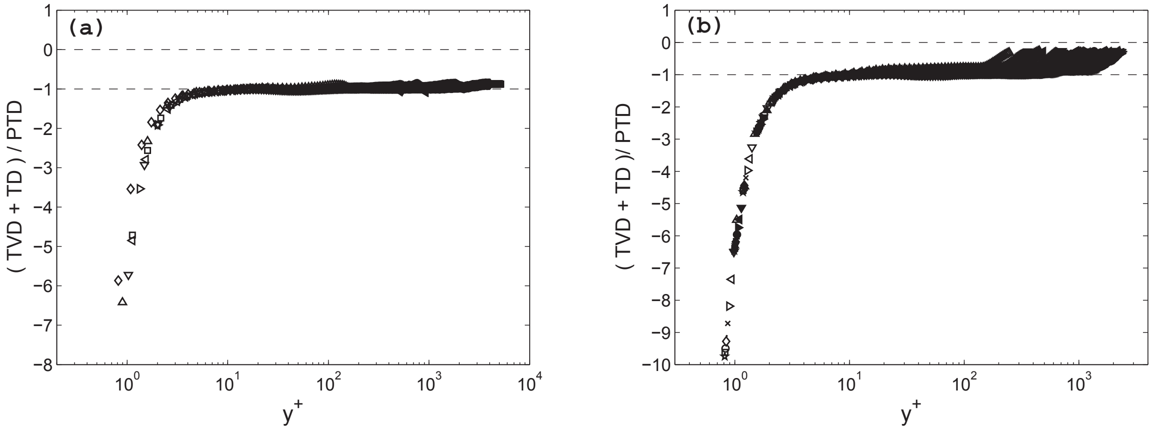

FIG. 14. Ratio of the sum of turbulent viscous diffusion and turbulent dissipation terms $(MVD + MD)$ to the production/turbulent diffusion term (PTD). (a) Channels. (b) Boundary layers. Symbols are the same as in Fig. 2.

this normalization does not alter conclusions regarding the resulting layer structure.

With $K^+ = 1/2\left\langle u_i^+ u_i^+ \right\rangle$, $T^+ = -\left\langle u^+ v^+ \right\rangle$, and by collecting terms, the inner-normalized budget equation for the turbulence kinetic energy in channel flow becomes

$$\frac{\partial^2}{\partial y^{+2}}\left(K^+\right) + \left[T^+ \frac{\partial U^+}{\partial y^+} - \frac{\partial}{\partial y^+}\left\langle v^+ K^+ \right\rangle\right] + d^+ + \frac{1}{\delta^+}\left[-\frac{\partial}{\partial y^+}\left\langle p^+ v^+ \right\rangle\right] = 0. \qquad \text{(A4)}$$

Four grouped terms in Eq. (A4) are referred to as turbulent viscous diffusion (TVD), production/turbulent diffusion (PTD), turbulent dissipation (TD) and turbulent pressure diffusion (TPD). The inner-normalized form of the turbulence kinetic energy budget for fully developed turbulent pipe flow has a form that is identical to that for channel flow when expressed in terms of the wall-normal variable $y^+ = \delta^+ - r^+$.

2. Boundary layer flow

Similar to the mean kinetic energy equation for the boundary layer, the advection of the turbulence kinetic energy can be written as

$$U_k \frac{\partial}{\partial x_k}\left[\frac{1}{2}\left\langle u_i u_i \right\rangle\right] = U \frac{\partial}{\partial x}\left[\frac{1}{2}\left\langle u_i u_i \right\rangle\right] + V \frac{\partial}{\partial y}\left[\frac{1}{2}\left\langle u_i u_i \right\rangle\right]. \qquad \text{(A5)}$$

The inner-normalized equation for the turbulent boundary layer then becomes

$$\frac{\partial^2}{\partial y^{+2}}\left(K^+\right) + \left[T^+ \frac{\partial U^+}{\partial y^+} - \frac{\partial}{\partial y^+}\left\langle v^+ K^+ \right\rangle\right] + d^+ + \left[-U^+ \frac{\partial}{\partial x^+} K^+ - V^+ \frac{\partial}{\partial y^+} K^+ - \frac{1}{\delta^+}\frac{\partial}{\partial y^+}\left\langle p^+ v^+ \right\rangle\right] = 0. \qquad \text{(A6)}$$

The first three grouped terms in Eq. (A7) are the same as in Eq. (A4). The fourth one is referred to as turbulent advection/pressure diffusion $(TAPD)$.

The leading balances for the turbulence kinetic energy (Eqs. A4 and A7) are considered, as these are useful for understanding the total budget structure. Here the results of Fig. 2 motivate examining the ratio of the sum of turbulent viscous diffusion and turbulent dissipation terms $(TVD + TD)$ to the production/turbulent diffusion term (PTD). Because the pipe flow results are essentially indistinguishable from the channel results, Fig. 14 only shows these ratio profiles for the channel and boundary layer. In contrast to the ratio profiles of the mean kinetic energy terms in Fig. 2, there is no apparent change of balance indicated in Fig. 14. The profile curves start from large negative values near the wall. Here Eqs. A4 and A7 indicate that the diffusion of TKE identically balances turbulent dissipation at the wall, and thus to leading order a small distance from the wall. Beyond this region, the ratio of Fig. 14 closely approximates -1. Detailed examination (not shown) indicates that this balance is comprised of one of the PTD terms and the TVD and TD terms. Along the -1 dashed line, the TVD term gradually gets closer to 0, which results in the change in balance from three terms to two terms; namely the TD and PTD terms. This two-term balance is continuously sustained throughout the remainder of the channel. Unlike the channel, the boundary layer profiles deviate from -1 and approach zero as $y \to \delta$. In this region, the $TAPD$ term increases in relative importance and forms a new balance with the TD and PTD terms. Thus, the turbulence kinetic energy budget exhibits three layers but four distinct balances in the boundary layer.

Appendix B: Turbulent pressure normalization

As described in Appendix A, in the present analysis turbulent pressure is effectively normalized by $\rho u_\tau \nu/\delta$, rather than by ρu_τ^2. If ρu_τ^2 is used for turbulent pressure normalization, the turbulent pressure diffusion term is simply given by $-\partial \langle p^+ v^+\rangle / \partial y^+$, and the normalized magnitude of this term increases by a factor of δ^+. This appendix quantifies, however, that the leading order balances do not change owing to the present choice for fluctuating pressure normalization.

Figs. 15 (a) and (b) show the ratio of $-\partial \langle p^+ v^+\rangle / \partial y^+$ to D^+. In layer i, all its values fall between 0 and -0.02, and thus the dominant balance determined for layer i herein is retained. In layer ii,$-\partial \langle p^+ v^+\rangle / \partial y^+$ is always observed to be less than 1/10 of the sum of the VD and D terms, and generally much less. This behavior is shown in Figs. 15 (c) and (d) for two representative Reynolds numbers. There is no apparent Reynolds number trend associated with this ratio. Across layers iii and iv the total pressure diffusion contribution in channel flows (or the advection/turbulent pressure diffusion in boundary layers) is still much larger than the turbulent pressure diffusion contribution. The profiles of Figs. 15 (e) and (f) at a fixed Reynolds number reflect representative behavior in this regard.

Appendix C: Basis for the characteristic length scale of layer iii

This appendix provides a scaling analysis for the channel supporting the use of the coordinate $(\delta^+ - \sqrt{\delta^+})$ used in a number of the figures herein. Eq. (17) reflects the relevant balance in layer iii. Note also that this layer is located in the inertial sublayer associated with the self-similarity admitted by the mean momentum equation [11]. Here, the normalized derivative of the turbulent inertia term, $A = -\partial^2 T^+/\partial y^{+2} \left(\partial T^+/\partial y^+ + 1/\delta^+\right)^{-3/2}$, approaches constancy as $\delta^+ \to \infty$ [34]. Given this condition, integration yields

$$\begin{aligned}\frac{\partial T^+}{\partial y^+} &= \left(\frac{2}{A}\right)^2 \left[\frac{1}{(y^+ - C)^2} - \frac{1}{\left(y_m^+ - C\right)^2}\right] \\ &= \frac{\phi^2}{(y^+ - C)^2} - \frac{\phi^2}{\left(y_m^+ - C\right)^2},\end{aligned} \tag{C1}$$

where $\phi = 2/A$, C is a constant, and T^+ attains its maximum value, T_m^+, at the position y_m^+. Integration of Eq. (C1) gives

$$T^+ = C' - \frac{\phi^2}{y^+ - C} - \frac{y^+\phi^2}{\left(y_m^+ - C\right)^2}, \tag{C2}$$

where $C' \to 1$ as $\delta^+ \to \infty$. The position of T_m^+ is empirically and asymptotically verified to be $y_m^+ = \lambda_m \sqrt{\delta^+}$, [34–36] where $\lambda_m \to \phi$ as $\delta^+ \to \infty$. Neglecting C for large δ^+ and using $y_m^+ = \lambda_m \sqrt{\delta^+}$ gives

$$\frac{\partial T^+}{\partial y^+} = \frac{\phi^2}{y^{+2}} - \frac{\phi^2}{\lambda_m^2 \delta^+}, \tag{C3}$$

and

$$T^+ = C' - \frac{\phi^2}{y^+} - \frac{y^+\phi^2}{\lambda_m^2 \delta^+}. \tag{C4}$$

The first term in Eq. (A3) can be expanded into two parts, e.g., $U^+\left(\partial T^+/\partial y^+\right)$ and $T^+\left(\partial U^+/\partial y^+\right)$. Each of these two terms is of the same order of magnitude as the last term, $\epsilon^2 U^+$. Letting $U^+\left(\partial T^+/\partial y^+\right) \sim \epsilon^2 U^+$(‘$\sim$’ denoting same order of magnitude) gives

$$\frac{\partial T^+}{\partial y^+} = O\left(\epsilon^2\right). \tag{C5}$$

This derivative magnitude is consistent with classical outer scaling arguments [12], and the momentum equation analyses of Wei *et al.* [20]. Specifically, $\partial T^+/\partial y^+$ becomes $O\left(\epsilon^2\right)$ at the beginning of layer III and retains this order of magnitude throughout both layers III and IV of the momentum balance. From Eq. (C3), we thus have

$$\frac{\phi^2}{y^{+2}} - \frac{\phi^2}{\lambda_m^2 \delta^+} = O\left(\epsilon^2\right). \tag{C6}$$

As $\delta^+ \to \infty$, $\phi \to \phi_c$ and $\lambda_m \to \phi_c$, where ϕ_c is a constant. Thus ϕ^2/λ_m^2 is $O(1)$, and ϕ_c^2 itself is an $O(1)$ constant. Under these conditions, Eq. (C6) is only valid when $y^+ \geqslant O(1/\epsilon)$. Requiring $y^+ \geqslant O(1/\epsilon)$ in Eq. (C4) and noting that $C' \to 1$ as $\delta^+ \to \infty$ yields

$$T^+ = O(1 - \epsilon). \tag{C7}$$

This order of magnitude is corroborated by the relevant region residing beyond the peak of T^+, where the maximum value T_m^+ is $1 - O(\epsilon)$ at y_m^+ [34].

Within layer iii, a rescaling of Eq. (A3) is now applied such that all terms reflect the actual orders of magnitude. The present analysis only requires considering the leading order balance between $\partial\left[U^+T^+\right]/\partial y^+$ and $\epsilon^2 U^+$. Rescaling begins by setting

$$U^+ = \alpha\bar{U}, \qquad T^+ = \beta\bar{T}, \qquad y^+ = y_0^+ + \gamma\bar{y}, \tag{C8}$$

where $\bar{U}$, $\bar{T}$ and $\bar{y}$ are all $O(1)$ as $\delta^+ \to \infty$. Analogous to y_m relative to layer III, y_0^+ is the position where the $\partial\left[U^+T^+ - \langle v^+K^+\rangle\right]/\partial y^+$ term changes sign in layer iii. The indicated transformations give

$$\frac{\partial}{\partial y^+}\left[U^+T^+\right] = \frac{\alpha\beta}{\gamma}\frac{\partial}{\partial \bar{y}}\left[\bar{U}\bar{T}\right], \qquad \epsilon^2 U^+ = \epsilon^2\alpha\bar{U}. \tag{C9}$$

Rendering all terms $O(1)$ requires that

$$\frac{\alpha\beta}{\gamma} = \epsilon^2\alpha, \tag{C10}$$

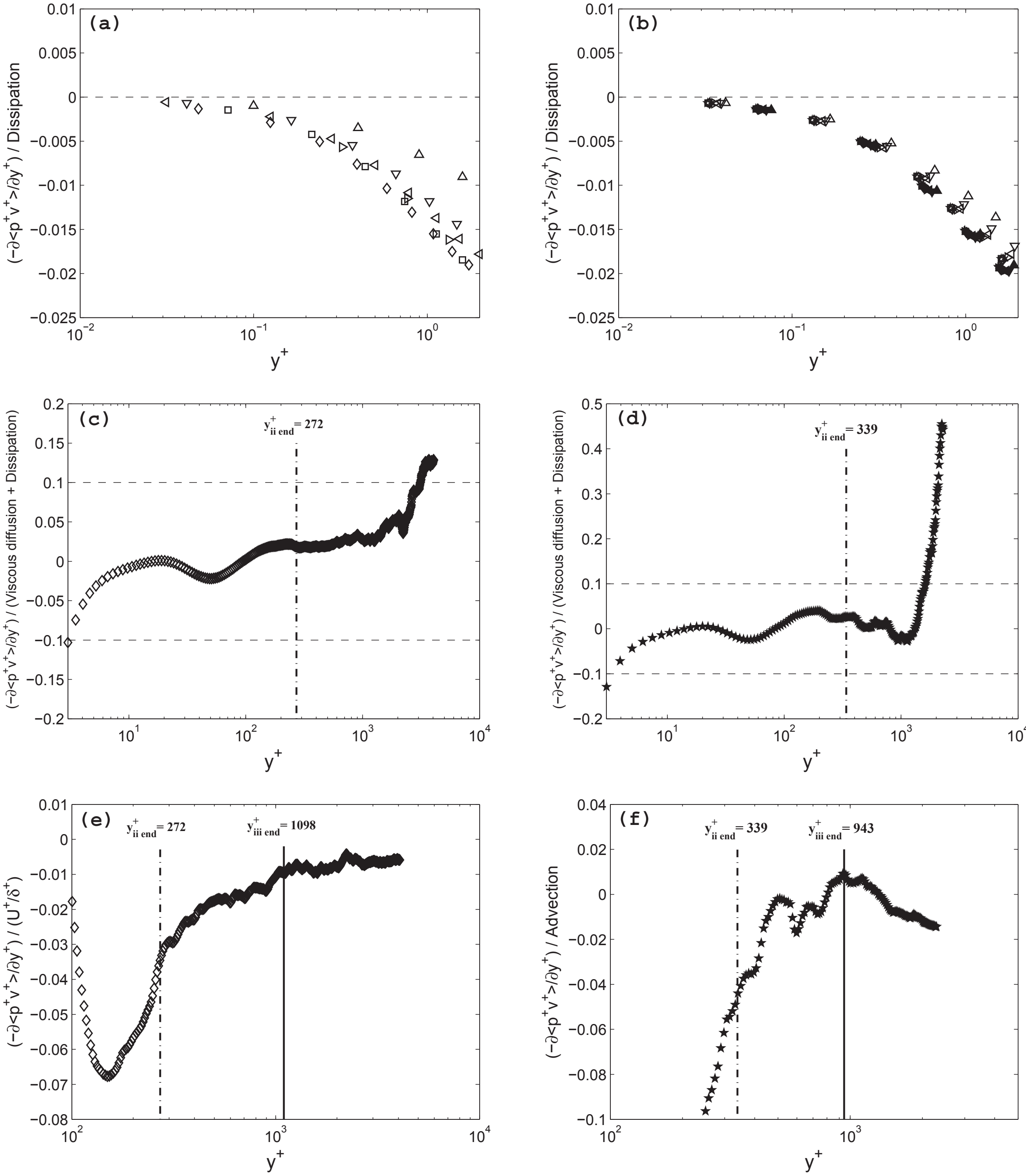

FIG. 15. Ratio of $-\partial\left\langle p^+v^+\right\rangle/\partial y^+$ to D term in layer i for (a) channels; (b)boundary layers. Ratio of $-\partial\left\langle p^+v^+\right\rangle/\partial y^+$ to the sum of the VD and D terms for (c) channel at $\delta^+ = 4079$; (d) boundary layer at $\delta^+ = 2299$. (e) Ratio of $-\partial\left\langle p^+v^+\right\rangle/\partial y^+$ to the mean pressure diffusion term for channel at $\delta^+ = 4079$; (f) Ratio of $-\partial\left\langle p^+v^+\right\rangle/\partial y^+$ to the advection term for boundary layer at $\delta^+ = 2299$.

or

$$\gamma = \frac{1}{\epsilon^2}\beta. \tag{C11}$$

From Eqs. (C7) and (C8) $\beta = 1 - \epsilon$ in layer iii, and with this γ is determined by

$$\begin{aligned}\gamma &= \frac{1}{\epsilon^2}\left(1-\epsilon\right)\\ &= \frac{1}{\epsilon^2} - \frac{1}{\epsilon},\end{aligned} \tag{C12}$$

or

$$\begin{aligned} y^+ &= y_0 + \left(\frac{1}{\epsilon^2} - \frac{1}{\epsilon}\right)\bar{y} \\ &= y_0 + (\delta^+ - \sqrt{\delta^+})\bar{y}. \end{aligned} \tag{C13}$$

By definition, $\bar{y}$ is $O\,(1)$ in layer iii, and thus it follows that the inner-normalized width of this layer is $O(\delta^+ - \sqrt{\delta^+})$. This scaling is interpreted as a finite Reynolds number correction to traditional outer scaling, since it is apparent that $(\delta^+ - \sqrt{\delta^+}) \to \delta^+$ as $\delta^+ \to \infty$.

[1] A.J. Smits, B.J. McKeon, and I. Marusic. High-reynolds number wall turbulence. *Ann. Rev. Fluid Mech.*, 43:353, (2011).

[2] I. Marusic, B.J. McKeon, P.A. Monkewitz, H.M. Nagib, A.J. Smits, and K.R. Sreenivasan. Wall-bounded turbulent flows at high Reynolds numbers: Recent advances and key issues. *Phys. Fluids*, 22(6):065103, (2010).

[3] J.C. Klewicki. Reynolds number dependence, scaling, and dynamics of turbulent boundary layers. *J. Fluids Eng.*, 132:094001, (2010).

[4] A.E. Perry and M.S. Chong. On the mechanism of wall turbulence. *J. Fluid Mech.*, 119:173, (1982).

[5] A.E. Perry and I. Marušic. A wall-wake model for the turbulence structure of boundary layers. part 1. extension of the attached eddy hypothesis. *J. Fluid Mech.*, 298:361, (1995).

[6] I. Marusic, J.P. Monty, M. Hultmark, and A.J. Smits. On the logarithmic region in wall turbulence. *J. Fluid Mech.*, 716:R3, (2013).

[7] C. Meneveau and I. Marusic. Generalized logarithmic law for high-order moments in turbulent boundary layers. *J. Fluid Mech.*, 719:R1, (2013).

[8] J. Klewicki, P. Fife, and T. Wei. On the logarithmic mean profile. *J. Fluid Mech.*, 638:73, (2009).

[9] A. Zhou and J. Klewicki. Properties of the streamwise velocity fluctuations in the inertial layer of turbulent boundary layers and their connection to self-similar mean dynamics. *Int. J. Heat Fluid Flow*, 51:372, (2015).

[10] J.C. Klewicki, C.T. Morrill-Winter, and A. Zhou. Inertial logarithmic layer properties and self-similar mean dynamics. *TSFP-9*, 3A:4, (2015).

[11] J.C. Klewicki. Self-similar mean dynamics in turbulent wall flows. *J. Fluid Mech.*, 718:596, (2013).

[12] H. Tennekes and J.L. Lumley. *A first course in turbulence*. MIT Press, (1972).

[13] S.B. Pope. *Turbulent flows*. Cambridge university press, (2000).

[14] P. Davidson. *Turbulence: An introduction for scientists and engineers*. Oxford University Press, USA, (2015).

[15] J. Laufer. *Investigation of turbulent flow in a two-dimensional channel*. NACA Rep. 1053, (1951).

[16] J. Laufer. *The structure of turbulence in full developed pipe flow*. NACA Rep. 1174, (1954).

[17] P.S. Klebanoff. *Characteristics of turbulence in a boundary layer with zero pressure gradient*. NACA Rep. 1247, (1955).

[18] H. Tennekes and J.L. Lumley. *The structure of turbulent shear flow*. Cambridge University Press, (1976).

[19] P. Fife, T. Wei, J. Klewicki, and P. McMurtry. Stress gradient balance layers and scale hierarchies in wall-bounded turbulent flows. *J. Fluid Mech.*, 532:165, (2005).

[20] T. Wei, P. Fife, J. Klewicki, and P. McMurtry. Properties of the mean momentum balance in turbulent boundary layer, pipe and channel flows. *J.Fluid Mech.*, 522:303, (2005).

[21] J.C. Klewicki. A description of turbulent wall-flow vorticity consistent with mean dynamics. *J. Fluid Mech.*, 737:176, (2013).

[22] P. Fife, J. Klewicki, P. McMurtry, and T. Wei. Multiscaling in the presence of indeterminacy: wall-induced turbulence. *Multiscale Model. Simul.*, 4(3):936, (2005).

[23] N.N. Mansour, J. Kim, and P. Moin. Reynolds-stress and dissipation-rate budgets in a turbulent channel flow. *J. Fluid Mech.*, 194:15, (1988).

[24] P.R. Spalart. Direct simulation of a turbulent boundary layer up to $R_\theta = 1410$. *J. Fluid Mech.*, 187:61, (1988).

[25] R.A. Antonia and J. Kim. Low-Reynolds-number effects on near-wall turbulence. *J. Fluid Mech.*, 276:61, (1994).

[26] R.D. Moser, J. Kim, and N.N. Mansour. Direct numerical simulation of turbulent channel flow up to $Re = 590$. *Phys. Fluids*, 11(4):943, (1999).

[27] G.N. Coleman, J. Kim, and P.R. Spalart. Direct numerical simulation of a decelerated wall-bounded turbulent shear flow. *J. Fluid Mech.*, 495:1, (2003).

[28] S. Hoyas and J. Jiménez. Reynolds number effects on the Reynolds-stress budgets in turbulent channels. *Phys. Fluids*, 20:101511, (2008).

[29] M. Bernardini, S. Pirozzoli, and P. Orlandi. Velocity statistics in turbulent channel flow up to $Re_\tau = 4000$. *J. Fluid Mech.*, 742:171, (2014).

[30] M. Lee and R.D. Moser. Direct numerical simulation of turbulent channel flow up to $Re_\tau = 5200$. *J. Fluid Mech.*, 774:395, (2015).

[31] G. Eitel-Amor, R. Örlü, and P. Schlatter. Simulation and validation of a spatially evolving turbulent boundary layer up to $Re_\theta = 8300$. *Int. J. Heat Fluid Flow*, 47:57, (2014).

[32] G.K. El Khoury, P. Schlatter, A. Noorani, P.F. Fischer, G. Brethouwer, and A. V. Johansson. Direct numerical simulation of turbulent pipe flow at moderately high Reynolds numbers. *Flow Turbulence Combust.*, 91:475, 2013.

[33] J. Elsnab, J. Klewicki, D. Maynes, and T. Ameel. Mean dynamics of transitional channel flow. *J. Fluid Mech.*, 768:451, (2011).

[34] J. Klewicki, J. Philip, I. Marusic, K. Chauhan, and C. Morrill-Winter. Self-similarity in the inertial region of wall turbulence. *Phys. Rev. E*, 90:063015, (2014).

[35] R.R. Long and T.-C. Chen. Experimental evidence for the existence of the mesolayerin turbulent systems. *J. Fluid Mech.*, 105:19, (1981).

[36] N. Afzal. Fully developed turbulent flow in a pipe: an intermediate layer. *Ingenieur-Archiv.*, 52(6):355, (1982).